RSC Advances

PAPER

View Article Online
View Journal | View Issue

Cite this: *RSC Adv.*, 2020, **10**, 10067

One-step synthesis of green emission carbon dots for selective and sensitive detection of nitrite ions and cellular imaging application†

Minghui Zan, ‡[ad] Cong Li,‡[c] Fei Liao,‡[a] Lang Rao,[a] Qian-Fang Meng,[a] Wei Xie,[a] Bei Chen,[a] Xingwang Qie,[b] Li Li,[b] Liang Wang,*[c] Wen-Fei Dong *[b] and Wei Liu *[ad]

In recent years, carbon dot (CD)-based fluorescent sensors for selective ions or small biomolecules have drawn great attention. In this work, highly fluorescent CDs (QY = 21%) were prepared from 2,3-diamino pyridine as the precursor through a facile solvothermal process. The CDs showed high stability and a green emission in aqueous, and the optimal emission wavelength of CDs is 508 nm under the excitation wavelength of 438 nm. Interestingly, a CDs-based nanoprobe was developed for a selective and sensitive fluorescence quenching response to NO_2^- in water, and the quenching mechanism was investigated in the work. Besides, the recovery rates of NO_2^- in the range of 98–103.5% were found to be acceptable, indicating that the proposed CDs could be act as potential candidates for determination of nitrite ions in real samples. Meanwhile, the nanoprobe was also successfully employed in a visualization biosensing platform for determination of NO_2^- in living cells due to its eminent biocompatibility.

Received 30th December 2019
Accepted 2nd March 2020

DOI: 10.1039/c9ra11009g

rsc.li/rsc-advances

1. Introduction

Nitrite ions (NO_2^-) are an important signal molecule in normal physiological activities, such as cell signalling, blood flow regulation and many other biological processes.[1,2] Whereas, excessive intake of nitrite ions with food or water can seriously endanger human health, due to its ability to interact with proteins and amines to produce carcinogenic nitrosamines which can lead to a variety of deformities and cancer. In addition, the presence of NO_2^- in synthetic urine could be used as an indicator of urinary tract infections.[3] In terms of the guideline of the World Health Organization, the maximum limit of nitrite in drinking water is <65 μM (or 3.0 mg mL^{-1}).[4] Up to now, a large number of analytical methods have been developed for quantitative analysis of NO_2^- in the aquatic environment, such as chromatography,[5] colorimetry,[6] capillary electrophoresis,[7] spectrophotometry[8] and electrochemical.[9–13] However, among them, some methods usually involve precision instruments, time-consuming and high costs. Therefore, developing more novel low-cost and nontoxic fluorescent materials for efficiency determination of nitrite is very important.

Carbon dots (CDs) as promising carbon nanomaterial have attracted extensive attention owing to their excellent fluorescence properties over the last decade.[14] Compared to traditional materials include of semiconductor quantum dots and organic fluorophores, CDs have some prominent merits such as ease fabrication, easy surface functionalization, low cytotoxicity, good stability and high biocompatibility, which enable them to show great potential applications in biosensing, bioimaging, drug delivery and photocatalysis.[15–21] On the other hand, most carbon dots are blue emitting and suffer from low quantum yield (QY), which limit their availability for applications. Recently, CDs-based fluorescent nanoprobes have been successfully applied to the analysis of metal ions including Fe^{3+}, Al^{3+}, Hg^{2+} and Cu^{2+}.[22–26] As for the detection of nitrite ions using CDs-based fluorescent sensors, there are a small number of studies reported.[27–29] Therefore, it is still a challenging task to exploring of low cost, favourable sensitive and selective sensors based on CDs for the detection of nitrite ions.

In this paper, we synthesized green fluorescent carbon dots by a facile solvothermal protocol. As shown in the Scheme 1, CDs with a high fluorescence quantum yield (21%) were synthesized using 2,3-diamino pyridine as raw materials and DMF as the solvent. Meanwhile, the resulting CDs can be

[a]*Key Laboratory of Artificial Micro- and Nano-Structures of Ministry of Education, School of Physics and Technology, Wuhan University, Wuhan, Hubei 430072, China. E-mail: wliu@whu.edu.cn*

[b]*CAS Key Laboratory of Bio-Medical Diagnostics, Suzhou Institute of Biomedical Engineering and Technology, Chinese Academy of Sciences, Suzhou, Jiangsu 215163, China. E-mail: wenfeidong@126.com*

[c]*College of Life Science and Technology, Xinjiang University, Xinjiang 830046, China*

[d]*Shenzhen Research Institute of Wuhan University, Shenzhen, Guangdong 518057, China*

† Electronic supplementary information (ESI) available. See DOI: 10.1039/c9ra11009g

‡ These authors contributed equally to this work.

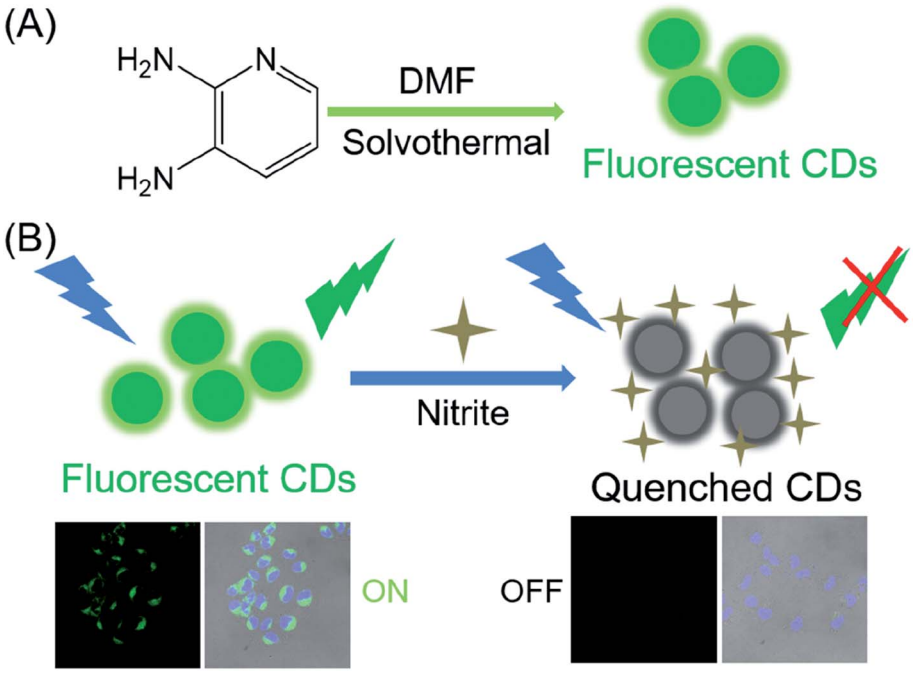

Scheme 1 (A) Schematic route of the carbon dots using 2,3-diamino pyridine precursors; (B) schematic illustration of fabricated CDs for NO_2^- detection.

applied to selectively detect NO_2^- in aqueous media, achieving an analytical detection limit of 2.8 nM. Practical applications for human urine, serum and water testing were successfully demonstrated. Thus, the presented fluorescent nanoprobe can be a promising sensing platform for nitrite ions analysis.

2. Experiment section

2.1. Materials

2,3-Diamino pyridine (PDA) was bought from Aladdin Reagent Company (Shanghai, China). Sodium nitrite, *N*,*N*-dimethylformamide (DMF) and Rhodamine 6G (99%) were purchased from Sinopharm Chemical Reagent Co. Ltd (Shanghai, China). All the chemicals were analytically pure and used without further purification. Deionized water (18.2 MΩ cm resistivity) was used throughout this study. Trypsin, Fetal bovine serum (FBS) and Dulbecco modified Eagle medium (DMEM) were ordered from GIBCO. DAPI and 3-(4,5-dimethylthiazol)-2,5-diphenyltetrazolium bromide (MTT) were ordered from Beyotime Institute of Biotechnology (Shanghai, China). HeLa cells and A549 cells were ordered from the Cell Bank of Chinese Academy of Sciences (Shanghai, China).

2.2. Characterizations

Cells imaging was performed on a Leica TCS SP5 microscope. Dynamic laser light scattering (DLS) measurements were conducted on a Malvern Zetasizer (Nano ZS90). Scattered light was collected at a fixed angle of 173° with a He–Ne laser (633 nm). A JEOL-2100F transmission electron microscope was employed to obtain transmission electron microscopy (TEM) experiments. The samples solutions (10 μL) were dropped onto a copper TEM grid and then dried overnight at room temperature. The UV/Vis absorption was determined with Agilent Cary 300 Scan UV-Vis spectrophotometer. The Raman spectra were collected on a Renishaw RM-1000 laser Raman microscope system. Infrared spectra (FT-IR) were obtained on an Agilent Cary 660 FTIR spectrometer. X-Ray photoelectron spectroscopy (XPS) measurements were carried out with an X-ray photoelectron spectrometer (AXIS ULTRA DLD). Photoluminescence spectra were performed on a Hitachi F-4600 fluorescence spectrophotometer. The fluorescent lifetime was measured by Edinburgh FLS1000 fluorescence spectrophotometer.

2.3. Preparation of carbon dots

The carbon dots (CDs) were facilely synthesized by solvothermal method. In a typical synthesis, 2,3-diamino pyridine (0.2 g) was dissolved in DMF solution (20 mL), after constant stirring, the solution was transferred into a poly(tetrafluoroethylene) (Teflon) liner stainless steel autoclave (50 mL) and heated at 180 °C for 10 hours. The autoclave was cooled down naturally. The solution of CDs was centrifuged for 15 minutes at medium speed (5000 rpm min^{-1}) to remove deposits. Then the clear solution was dialyzed (MWCO: 500 Da) against DI water to remove small molecules and unreacted reagent for 72 h. Finally, the obtained clear aqueous solution was freeze-dried to prepare the dry CDs product.

2.4. Fluorescence quantum yield measurement of carbon dots

To measure the quantum yield of as-prepared carbon dots in water, Rhodamine 6G was dissolved in ethanol (QY 95%) was

employed as standards. The quantum yield (QY) of CDs was obtained by the following comparative equation:

$$QY_S = QY_{ST}(A_{ST}/A_S)(I_S/I_{ST})(\eta_S/\eta_{ST})^2$$

where η indicates the refractive index of the solvent; I denotes the integrated emission intensity; A is the optical density (absorption); the subscript "ST" and "S" represent the standard (Rhodamine 6G) with a known QY and CDs, respectively. To obtain more reliable results and minimize the re-absorption effects, A_S and A_{ST} measured were kept below 0.10.

2.5. Fluorescent detection of NO_2^-

The concentration of carbon dots was 0.2 mg mL^{-1} in PBS solution. To evaluate the sensitivity of the nitrite ions determination, various concentrations of nitrite ions (0, 0.005, 0.01, 0.015, 0.02, 0.025, 0.03, 0.035, 0.04, 0.2, 1, 5, 10 and 40 μM) with 10 μL as-prepared CDs were added into 1 mL PBS buffer solutions (pH 7.4). To identify the selective detection performance for nitrite ions by the as-prepared carbon dots, we choose different ions (such as F^-, NO_3^-, Cl^-, SO_4^{2-}, Br^-, CO_3^{2-}, Ac^-, HCO_3^-, CN^-, $H_2PO_4^-$, SO_3^{2-}, PO_4^{2-}) instead of nitrite ions to record the fluorescence spectra as previously described. The final concentration of potential interfering substances was 10 μM, respectively. All the fluorescence spectra were measured from 450 nm to 700 nm ($\lambda_{ex} = 438$ nm) after incubated for 5 min before the spectral measurements. The sensitivity and selectivity experiments were performed at room temperature.

2.6. Cytotoxicity assay

The cytotoxicity of CDs was detected with HeLa cells and A549 cells using a standard MTT assay. Briefly, HeLa cells and A549 cells (density: 5000 cells per well) were seeded into 96-well plates and cultured in 100 μL DMEM under humidified 5% CO_2 atmosphere overnight. After removing incubation medium, followed by incubated with different concentrations of CDs for another 24 h. Thereafter, 20 μL of MTT medium (5 mg mL^{-1}) was added and then cultured at 37 °C for 4 hours. Finally, the medium was replaced with DMSO (200 μL) and shaken for 20 min to release blue formazan crystals. Finally, the absorbance of every well was measured by microplate reader at 490 nm.

2.7. Confocal laser scanning microscope studies

HeLa cells were used as the model for fluorescence imaging. Typically, HeLa cells in the DMEM medium with 10% FBS were cultured in each 35 mm glass-bottom culture dishes for 24 h. Then, the mixture of CDs (0.15 mg mL^{-1}) in DMEM medium (2 mL) was added into each dish and then incubated for another 12 h. Subsequently, the cells in each well were rinsed with ice-cold PBS to remove residual completely. Furthermore, different concentrations of nitrite ions (0 μM, 0.1 μM, 0.3 μM) were added and incubated for another 1 h. Finally, cells were washed with PBS three times, and cell nuclei were stained with DAPI for 10 min. The fluorescence images were observed under CLSM.

2.8. Detection of nitrite ions in real samples

In order to determine the feasibility of the as-prepared CDs nanoprobe for the NO_2^- detection, tap water, Taihu water (Suzhou, Jiangsu, China), human urine, and serum were chosen as models for environmental and biological, respectively. Water samples were filtered through 0.22 μm millipores prior to analysis. Fresh human urine samples were collected from healthy volunteer for the recovery experiment. The urine samples were subjected to centrifugation and diluted 20 times with 0.1 M PBS buffer solutions (pH 7.2). Serum samples were collected from the Suzhou Science & Technology Town Hospital. Serum samples were subjected to a 20-fold dilution before analysis. Real samples were spiked with the different concentrations of the corresponding nitrite ions and then added to the sensing system. Finally, the fluorescence of the mixture was measured by the fluorescence spectra.

3. Results and discussions

3.1. Synthesis and characterization of the as-prepared carbon dots

The water-soluble carbon dots synthesized *via* the solvothermal method as shown in Scheme 1. The synthetic conditions of carbon dots were explored in detail, including the heating time and temperature. In the end, the brown solution was acquired. As shown in Fig. 1A and B, the morphology and size of as-prepared CDs were investigated by DLS and TEM. The resulting carbon dots exhibited a hydrodynamic diameter of 4.7 nm. Meanwhile, TEM images of carbon dots show a uniform size with an average diameter of 1.5–4.8 nm, which was in good agreement with the DLS characterization results of CDs. The HR-TEM image in the inset of Fig. 1A shows that the as-prepared CDs possessed a crystalline structure with the lattice fringe spacing of 0.215 nm, which is consistent with the (002) lattice spacing of graphitic carbon.[30]

The structure and surface functional groups of CDs were characterized with Fourier transform infrared (FT-IR) spectra. In the FT-IR spectra (Fig. 1C), the peak at 3337 cm^{-1} was assigned to the O–H vibrations, and the absorption band at about 3193 cm^{-1} can be assigned to the stretching vibration of N–H.[31,32] Furthermore, the sharp peaks at 1620, 1455, 1395 and 1051 cm^{-1} were attributed to the C=C, C–H, N–H and C–N vibrations, respectively.[33–38] Furthermore, the surface potential of carbon dots in aqueous solution was confirmed by the zeta potentiometer, which is measured to be +5.95 mV. The positive charge of CDs might be attributed to the positively charged moieties (*e.g.* amine groups) on the surface of carbon dots. The above data indicate that the as-prepared CDs can be well dispersed in water because of the presence of N-related groups (*e.g.* –NH) and hydrophilic groups (*e.g.* –OH) on their surface. The Raman spectra of CDs in Fig. 1D reflect two major peaks at 1320 cm^{-1} and 1576 cm^{-1}, ascribed to the disordered structures or defects (D band), and graphitic carbon domains (G band) in carbon dots, respectively. The intensity ratios of D and G bands is 0.72, indicating a similar structure to graphite.[39]

Besides the FT-IR characterization, the elemental states and surface functionality of carbon dots were also determined by X-ray

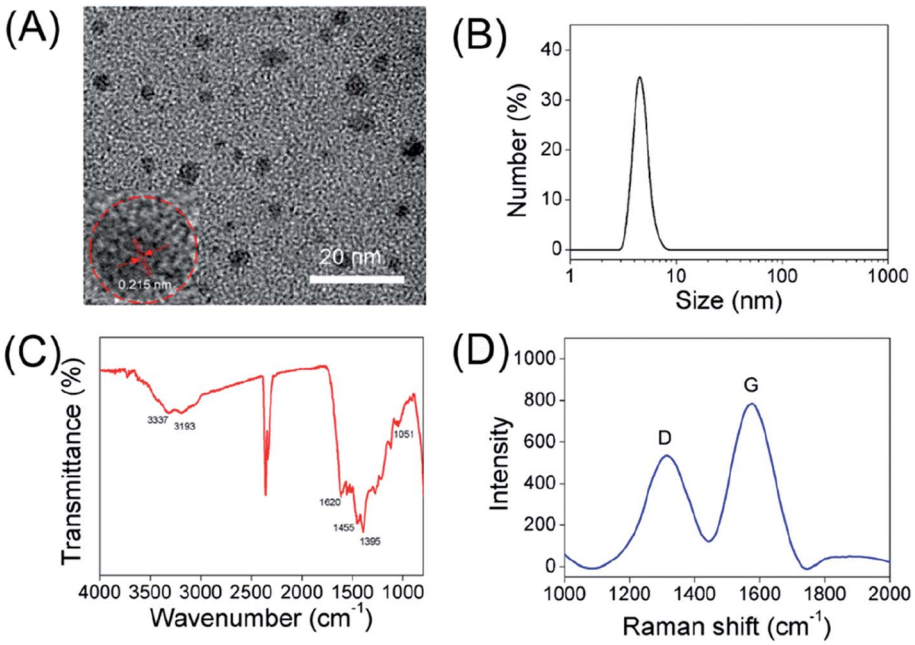

Fig. 1 (A) TEM images of the carbon dots. Inset: HRTEM lattice fringe image of CDs. (B) Number-averaged particle diameter from DLS of the as-fabricated CDs. (C) FT-IR spectra of the CDs. (D) Raman spectrum of CDs.

photoelectron spectroscopy (XPS). As displayed in Fig. 2A, there were three main peaks at 284, 399 and 530 eV, which represented C 1s, N 1s and O 1s, respectively. Furthermore, the elemental analysis results of the CDs were made up of carbon (66.09%), oxygen (4.3%) and nitrogen (29.6%). In detail, the C 1s spectrum (Fig. 2B) can be divided into five peaks at 283.9, 284.4, 285.9, 285.1 and 288.4 eV, which are ascribed to C=C, C–C, C–N, C–O and C=O bonds, respectively. As shown in the high-resolution O 1s spectra (Fig. 2C), the oxygen existed in three different states: C–O, C=O and C–O–C (530.3, 531.5 and 532.8 eV). In addition, the N 1s spectrum (Fig. 2D) of the carbon dots could be decomposed into four peaks such as pyridinic N (397.6 eV), amino N (398.2 eV), pyrrolic N (399.9 eV), and graphitic N (398.9 eV). These results established that the obtained CDs were doped with nitrogen and oxygen elements.

3.2. Optical properties of CDs

The UV-Vis absorption spectra of the as-prepared CDs, as shown in Fig. 3A, the band at 308 nm (originated from the n–π* transition

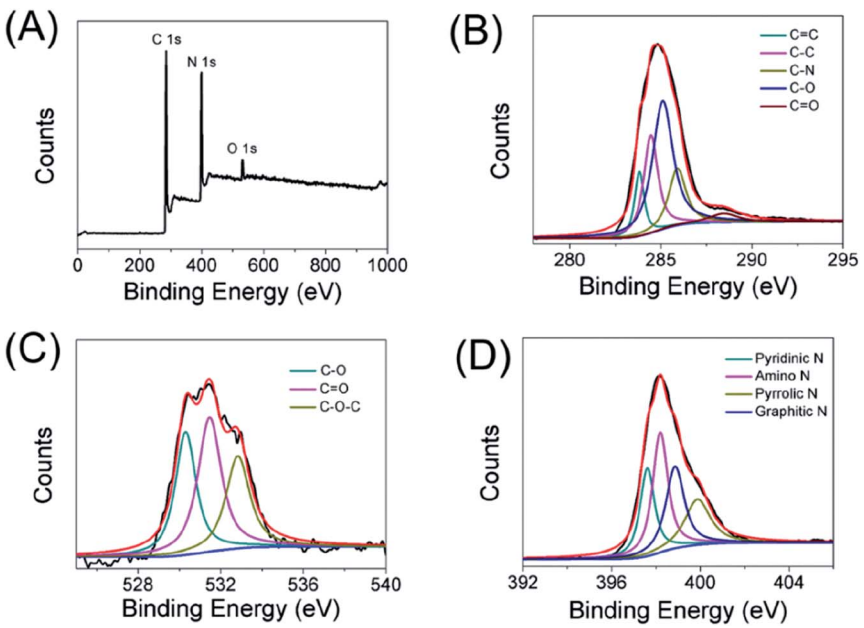

Fig. 2 XPS spectrum of the as-prepared carbon dots (A), high-resolution XPS spectra of C 1s (B), O 1s (C), N 1s (D) of the carbon dots, respectively.

of C=O group) along with a low energy absorption band at 415 nm because of π-conjugated structure and/or connected chemical groups of the as-prepared carbon dots. Moreover, the maximum excitation wavelength of the CDs is located at 438 nm, giving a maximum emission band characterized at $\lambda = 508$ nm (black curve and red curve in Fig. 3A, respectively). At the same time, the images of the obtained CDs taken under daylight and 365 nm UV lamp irradiation were inserted in Fig. 3A, showing a bright green fluorescence. In quest of further investigating the optical properties of carbon dots, the λ_{ex}-dependent photoluminescence (PL) behavior was researched and is displayed in Fig. 3B. Interestingly, when the excitation wavelength is increased from 360 to 460 nm, the red shift of fluorescence emission peaks of the CDs is small (the λ_{em} at around 500–515 nm) and only the FL intensity changes. The fluorescence emission of CDs correspond to the CIE color coordinate of (0.24, 0.52) (Fig. 3C), which further demonstrating the green emission of the CDs. In addition, the QY of the as-prepared carbon dots was calculated to be approximately 21% using Rhodamine 6G as a reference. All of these indicated that the as-prepared carbon dots have excellent optical performance, which is beneficial for applications in cellular imaging.

3.3. Fluorescence stability investigation

The fluorescent stability of as-prepared CDs under different conditions was investigated to examine their performance. As displayed in Fig. S1,† only a slight change in the fluorescence intensity was observed in the presence of NaCl solution with the concentration higher than 2.0 M, which revealed that the as-prepared carbon dots have excellent salt resistance even under high ionic strength conditions. Furthermore, the influence of pH values on the FL of the as-prepared carbon dots was also studied. As depicted in Fig. S2,† the fluorescence intensity keep stable (pH variation from 3 to 9) and decrease in higher pH solution or strong acidic solution. In addition, little decrease of FL is observed under continuous irradiation (365 nm) with a UV lamp, which implied that the carbon dots possess good photostability (Fig. S3†). At the same time, the CDs were stable when stored at 4 °C for 6 weeks (Fig. S4†). These results demonstrating the carbon dots have great potential for bioimaging and sensing applications under physiological conditions.

3.4. Selectivity and sensitivity analysis of the as-prepared CDs for nitrite ions detection

According to the superior optical properties (*e.g.* high photostability and bright green emission), the CDs was proposed to serve as a biological nanoprobe. Subsequently, the bio-nanoprobe was evaluated for nitrite ions sensing in PBS buffer. As depicted in Fig. 4A, the fluorescence intensity of CDs at 508 nm is gradually quenched along with the increasing concentration of nitrite ions form 0 to 40 μM. Obviously, over 80% fluorescence intensity was quenched after adding of nitrite ions at the concentration of 10 μM (Fig. S5†), fully demonstrating the feasibility of NO_2^- detection. The linear response of

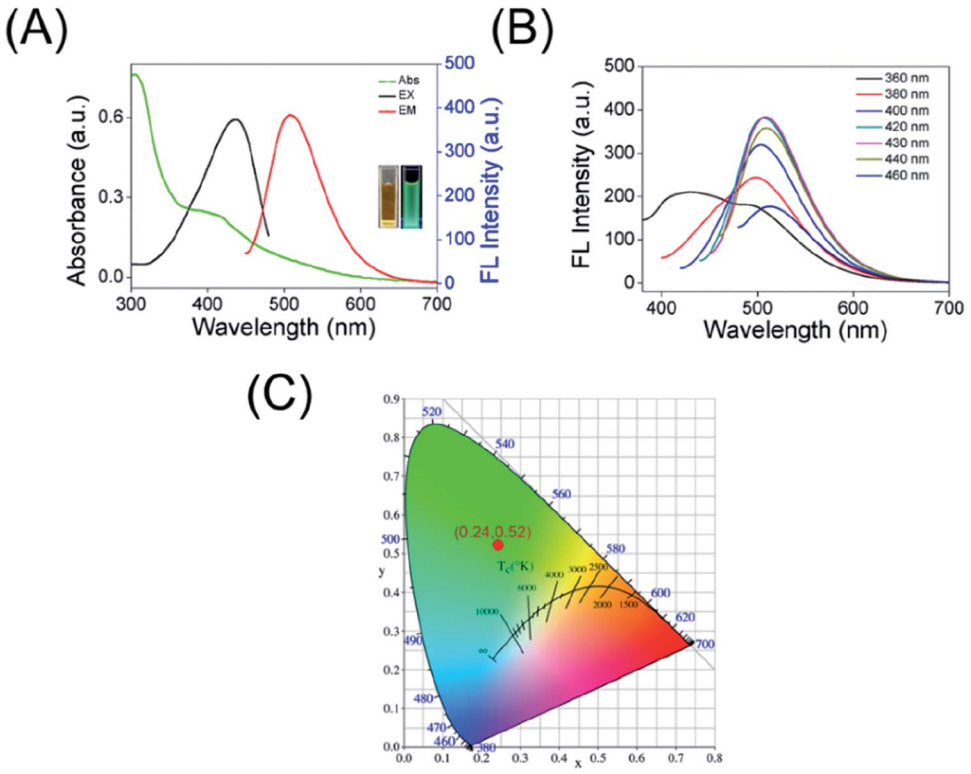

Fig. 3 (A) The normalized UV-Vis absorption spectra, FL emission and excitation spectra of the CDs. Inset: photographs of the CDs under the irradiation of the day light and UV lamp. (B) Fluorescent spectra under different excitation wavelengths of the carbon dots. (C) Calculated CIE color coordinates from the PL spectra of the CDs.

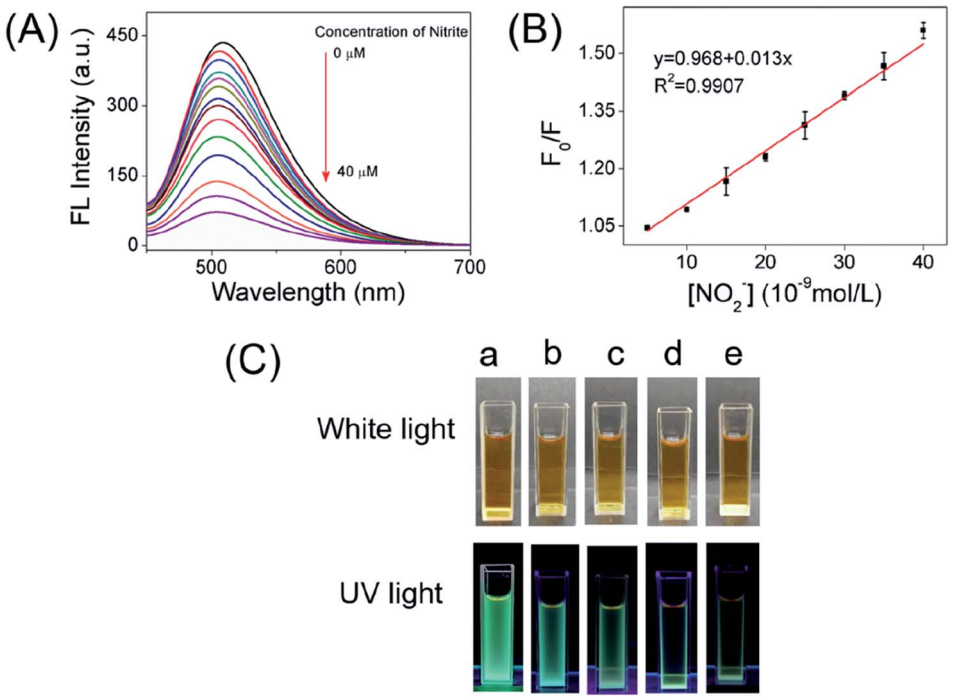

Fig. 4 (A) The fluorescence spectra of the as-prepared CDs by gradual addition of different amounts of NO_2^- (from top to bottom, respectively). (B) The correlation between fluorescence intensity and NO_2^- ions at the various concentrations of 5–40 nM. (C) Photographs of the corresponding samples (0.2 mg mL^{-1}) under daylight and UV light (a: 0 μM NO_2^-; b: 0.02 μM NO_2^-; c: 0.1 μM NO_2^-; d: 2 μM NO_2^-; e: 10 μM NO_2^-.).

F_0/F *versus* the concentration of nitrite ions in the range of 0.005–0.04 μM was obtained (Fig. 4B), where F_0 and F are the FL intensities of the as-prepared CDs in the absence and presence of NO_2^-. It is worth to point out that it displays a good linear with a correlation coefficient (R^2) of 0.9907. In addition, the limit of detection (LOD) for NO_2^- is determined to be 2.8 nM (signal/noise = 3). Compared with other reported works (Table S1†), the present nanoprobe based on CDs had a lower detection limit for the detection of nitrite ions. Besides, the present nanoprobe not only is reachable with fast, simple and low cost, but also possesses high capability and accuracy in diverse environments. Fig. 4C shows the naked eye photographic images of the corresponding CDs samples in the presence of nitrite with different concentrations under daylight and UV light, suggesting that the color changes induced by NO_2^-. These results showed that the proposed nanoprobe could be applied for the detection of NO_2^-.

In addition, in order to explore the fluorescence responses of the as-prepared CDs for NO_2^-, the FL of the carbon dots were investigated in the presence of various interference ions in aqueous solution. Fig. 5A displays the least FL intensity was observed in the presence of NO_2^- as compared to multiple interfering ions. This result clearly indicates that the emission of green-emitting CDs work as a nanoprobe for the detection of nitrite ions.

3.5. Fluorescence quenching mechanism

To better understand the fluorescence quenching mechanism of CDs, the time-dependent carbon dots fluorescence decay induced by nitrite ions was investigated by fluorescence lifetime spectroscopy. The average lifetimes were calculated according to the following equation:

$$\tau_{ave} = (A_1\tau_1^2 + A_2\tau_2^2)/(A_1\tau_1 + A_2\tau_2)$$

where A_1 and A_2 represent the relative weights of time-resolved fluorescence decay lifetimes τ_1 and τ_2, respectively.

As shown in Fig. 5B, the average fluorescence lifetime (τ_{ave}) of the obtained CDs was found to be 3.84 ns, consisting of two components: 1.24 ns (*ca.* 24.71%) and 4.1 ns (*ca.* 75.29%). After treatment with nitrite ions (40 nM), the average lifetime of CDs decreased to 3.71 ns, and consisted of two components: 1.46 ns (*ca.* 6.5%) and 3.77 ns (*ca.* 93.5%). This suggests a static fluorescence quenching process occurred.

To elucidate the quenching mechanism, we also calculated the quenching constant using the well-known Stern–Volmer equation:

$$F_0/F = 1 + K_{SV}[Q]$$

Wherein [Q] is the concentration of the quencher; K_{SV} is the quenching constant; F_0 and F are the fluorescence intensities in the absence and the presence of nitrite ions, respectively.

In this work, the low NO_2^- concentration (0.005–0.04 μM) was described by the Stern–Volmer equation with a good linear behavior, and the K_{SV} was calculated to be 1.4×10^7 M^{-1}, indicating the quenching mode is static quenching effect.[40,41]

Then, we studied the changes of the UV-Vis absorption spectra of carbon dots after the addition of nitrite, which only

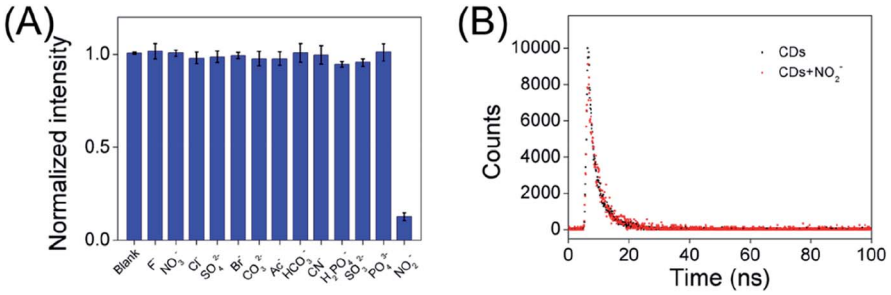

Fig. 5 (A) The normalized fluorescence quenching efficiency of the CDs after addition of multiple interfering ions. (B) Lifetimes of steady-state fluorescence of CDs and CDs + nitrite ions (40 nM).

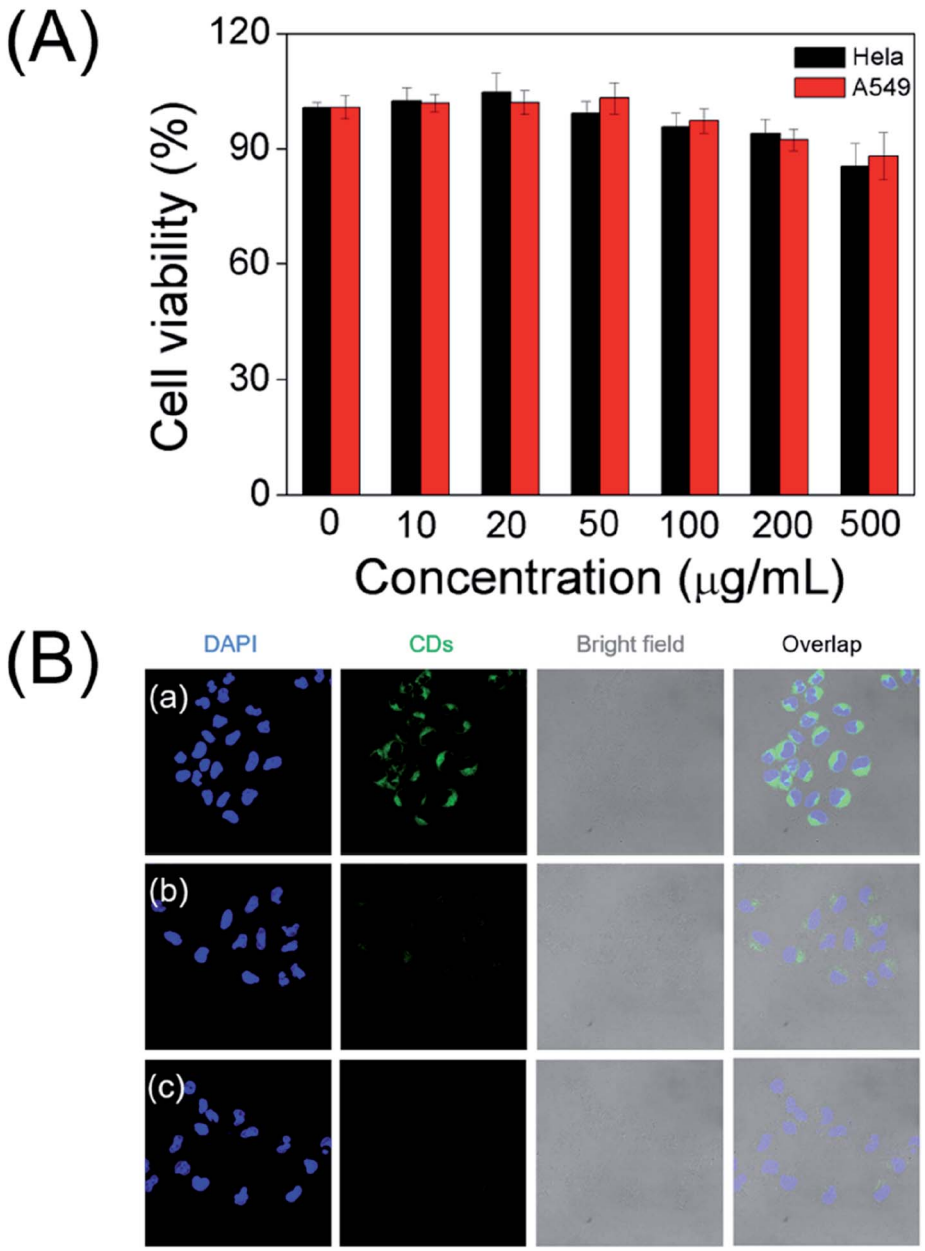

Fig. 6 (A) Cellular viability assessment of HeLa cells and A549 cells treated with carbon dots under various concentrations after 24 h incubation. (B) CLSM images of HeLa cells after incubation with CDs (a), CDs + 0.1 μM NO_2^- (b), CDs + 0.3 μM NO_2^- (c), respectively. DAPI (blue) was used to stain cell nucleus.

exhibited characteristic absorption peak of NO_2^- at 354 nm, and no other obvious change was found in the system (Fig. S6A†). The result further supported the static quenching mechanism.[42–44] From Fig. S6B,† when NO_2^- was added into carbon dots solution, the zeta potential value changed from 5.95 mV to −1.82 mV, indicating that the nitrite ions can be bounded on the surface of the CDs, and the positive charge as shielded. In addition, as can be seen in Fig. S7A,† TEM image showed that CDs aggregated in the presence of nitrite ions. The DLS (Fig. S7B†) experiments showed the hydrodynamic diameter of CDs changed essentially upon the introduction of nitrite ions. The high selectivity of the carbon dots towards nitrite ions could be that the interaction between nitrite ions and amine groups on the surface of CDs made the carbon dots close to each other, which probably resulted in electron transfer between CDs and NO_2^-.[45] Therefore, this is an indication of the possibility of aggregation-induced emission quenching. This deserves further investigation in our future work. Meanwhile, the electron transfer process between CDs and nitrite ions can explain the reason that passivated carbon dots shows higher LOD towards NO_2^-.

3.6. Biocompatibility study

To explore the as-prepared carbon dots for potential bioimaging application, the cellular cytotoxicity of the water soluble CDs was evaluated by the standard MTT colorimetric assay. After incubating HeLa cells and A549 cells with the CDs for 24 h, as depicted in Fig. 6A, the survival rates remained greater than 90% even at very high doses (500 μg mL^{-1}). The results suggest that the as-prepared CDs have low cytotoxicity and excellent biocompatibility.

3.7. Application of CDs in cellular imaging

Accordingly, living cells and CLSM images were executed to further prove their potential application in bioimaging. As shown in Fig. 6B, a noticeable green fluorescence was observed in the HeLa cells after incubating with CDs for 12 h at 37 °C. These results indicate that as-prepared carbon dots nanoprobe is capable to permeate into cells. As expected, the fluorescence brightness of the cells gradually weaken with the increase in the concentration of NO_2^-, supporting as-prepared carbon dots reacting with nitrite ions to produce discernible fluorescence signal in cells. These results demonstrate that the CDs could be applied for visually detection of nitrite ions in live cells.

3.8. Real samples analysis

To further determine the applicability in real samples, the synthesized CDs were applied to detect nitrite ions in tap water, Taihu water, human urine and serum. The recovered fluorescence variation test of the CDs induced by NO_2^- were applied and the results are shown in Table 1. It is obvious that the recoveries vary from 98% to 103.5%, and the relative standard deviations (RSD) are below 3%. The fluorescent nanoprobe could be effectively to determination of trace levels of NO_2^- ions in human blood and urine. The pretreatment procedure of samples and the establishment of the standard curve referenced to GB (5009.33-2016) of National food safety standard. The results (Fig. S8 and Table S2†) suggested that the CDs-based nanoprobe could be used for the selective detection of NO_2^- in real samples. Therefore, the results demonstrated that the as-prepared CDs showed an application potential for nitrite ions in real samples.

Table 1 Recovery experiments of NO_2^- from real samples

Samples	Added (nM)	Measured (nM)	Recovery (%)	RSD (%, $n = 5$)
Tap water 1	20	20.3	101.5	2.1
Tap water 2	40	39.3	98.2	1.7
Taihu water 1	20	19.7	98.5	2.1
Taihu water 2	40	40.4	101	1.6
Human urine 1	20	20.4	102	1.7
Human urine 2	40	41.4	103.5	2.9
Serum 1	20	19.6	98	2.0
Serum 2	40	39.7	99.2	1.4

4. Conclusions

In conclusion, we have successfully introduced a feasible and simple method to construct a fluorescent nanoprobe based on CDs for the sensitive and selective detection of NO_2^- ions. The CDs fabricated in this work exhibited favourable biocompatibility, bright green photo-luminescence, high fluorescence stability, as well as low-toxicity. In addition to the high sensitivity, the specificity to detect NO_2^- had been demonstrated against competing ions. Further studies revealed that the CDs had been used as promising fluorescent nanoprobe for bioimaging. Remarkably, practical applications for human urine, serum and water testing were successfully demonstrated. As a consequence, the as-prepared CDs has a great potential for nitrite ions detection in real samples and imaging in biological applications.

Author contributions

M. Z. and W. L. designed research; C. L., F. L., L. R., Q. M., W. X., B. C., X. Q. and L. L. performed research; M. Z., L. W. and W. D. analyzed data; and M. Z. and W. L. wrote the paper.

Ethics statement

All experiments were performed in accordance with the Guidelines "Biomedical research ethics review method involving people" (China), and approved by the ethics committee at Wuhan University. Informed consents were obtained from human participants of this study.

Conflicts of interest

The authors declare no competing financial interest.

Acknowledgements

The present work was supported by the National Research and Development Program for Major Research Instruments (Grant No. 81527801), the National Key Research and Development Program (2016YFC1000701), the Basic Research Projects of Shenzhen Knowledge Innovation Program (JCYJ20180302173424902), and the Frontier Projects of Applied Foundation in Wuhan (2019010701011386).

Notes and references

1 N. S. Bryan, B. O. Fernandez, S. M. Bauer, M. F. Garcia-Saura, A. B. Milsom, T. Rassaf, R. E. Maloney, A. Bharti, J. Rodriguez and M. Feelisch, *Nat. Chem. Biol.*, 2005, **1**, 290.
2 M. Gilchrist, A. C. Shore and N. Benjamin, *Cardiovasc. Res.*, 2011, **89**, 492–498.
3 C. He, B. D. Howes, G. Smulevich, S. Rumpel, E. J. Reijerse, W. Lubitz, N. Cox and M. Knipp, *J. Am. Chem. Soc.*, 2015, **137**, 4141–4150.
4 T. Ohno, M. Akiyoshi, T. Umebayashi, K. Asai, T. Mitsui and M. Matsumura, *Appl. Catal., A*, 2004, **265**, 115–121.
5 J. M. Doyle, M. L. Miller, B. R. McCord, D. A. McCollam and G. W. Mushrush, *Anal. Chem.*, 2000, **72**, 2302–2307.
6 T. M. G. Cardoso, P. T. Garcia and W. K. T. Coltro, *Anal. Methods*, 2015, **7**, 7311–7317.
7 X. Wang, E. Adams and A. Van Schepdael, *Talanta*, 2012, **97**, 142–144.
8 P. Li, Y. Ding, A. Wang, L. Zhou, S. Wei, Y. Zhou, Y. Tang, Y. Chen, C. Cai and T. Lu, *ACS Appl. Mater. Interfaces*, 2013, **5**, 2255–2260.
9 F. Xu, M. Deng, Y. Liu, X. Ling, X. Deng and L. Wang, *Electrochem. Commun.*, 2014, **47**, 33–36.
10 M. Saraf, R. Rajak and S. M. Mobin, *J. Mater. Chem. A*, 2016, **4**, 16432–16445.
11 C.-H. Su, C.-W. Kung, T.-H. Chang, H.-C. Lu, K.-C. Ho and Y.-C. Liao, *J. Mater. Chem. A*, 2016, **4**, 11094–11102.
12 S.-S. Li, Y.-Y. Hu, A.-J. Wang, X. Weng, J.-R. Chen and J.-J. Feng, *Sens. Actuators, B*, 2015, **208**, 468–474.
13 X. Luo, J. Pan, K. Pan, Y. Yu, A. Zhong, S. Wei, J. Li, J. Shi and X. Li, *J. Electroanal. Chem.*, 2015, **745**, 80–87.
14 S. Y. Lim, W. Shen and Z. Gao, *Chem. Soc. Rev.*, 2015, **44**, 362–381.
15 B. B. Chen, R. S. Li, M. L. Liu, H. Z. Zhang and C. Z. Huang, *Chem. Commun.*, 2017, **53**, 4958–4961.
16 S. Qu, D. Zhou, D. Li, W. Ji, P. Jing, D. Han, L. Liu, H. Zeng and D. Shen, *Adv. Mater.*, 2016, **28**, 3516–3521.
17 L. Wang, B. Li, F. Xu, X. Shi, D. Feng, D. Wei, Y. Li, Y. Feng, Y. Wang, D. Jia and Y. Zhou, *Biosens. Bioelectron.*, 2016, **79**, 1–8.
18 I. P.-J. Lai, S. G. Harroun, S.-Y. Chen, B. Unnikrishnan, Y.-J. Li and C.-C. Huang, *Sens. Actuators, B*, 2016, **228**, 465–470.
19 A. Jaiswal, S. S. Ghosh and A. Chattopadhyay, *Chem. Commun.*, 2012, **48**, 407–409.
20 C. Ding, A. Zhu and Y. Tian, *Acc. Chem. Res.*, 2014, **47**, 20–30.
21 M. Zheng, Z. Xie, D. Qu, D. Li, P. Du, X. Jing and Z. Sun, *ACS Appl. Mater. Interfaces*, 2013, **5**, 13242–13247.
22 Y. Zhu, M. Qiao, W. Peng, Y. Li, G. Zhang, F. Zhang, Y. Li and X. Fan, *J. Mater. Chem. A*, 2017, **5**, 9272–9278.
23 J. Shangguan, J. Huang, D. He, X. He, K. Wang, R. Ye, X. Yang, T. Qing and J. Tang, *Anal. Chem.*, 2017, **89**, 7477–7484.
24 L. Shi, L. Li, X. Li, G. Zhang, Y. Zhang, C. Dong and S. Shuang, *Sens. Actuators, B*, 2017, **251**, 234–241.
25 A. Kumari, A. Kumar, S. K. Sahu and S. Kumar, *Sens. Actuators, B*, 2018, **254**, 197–205.
26 X. Qie, M. Zan, P. Miao, L. Li, Z. Chang, M. Ge, P. Gui, Y. Tang and W.-F. Dong, *J. Mater. Chem. B*, 2018, **6**, 3549–3554.
27 M. Zan, L. Rao, H. Huang, W. Xie, D. Zhu, L. Li, X. Qie, S.-S. Guo, X.-Z. Zhao, W. Liu and W.-F. Dong, *Sens. Actuators, B*, 2018, **262**, 555–561.
28 H. Zhang, S. Kang, G. Wang, Y. Zhang and H. Zhao, *ACS Sens.*, 2016, **1**, 875–881.
29 R. Liu, J. Zhao, Z. Huang, L. Zhang, M. Zou, B. Shi and S. Zhao, *Sens. Actuators, B*, 2017, **240**, 604–612.
30 H. Li, Z. Kang, Y. Liu and S.-T. Lee, *J. Mater. Chem.*, 2012, **22**, 24230–24253.
31 Z. L. Wu, M. X. Gao, T. T. Wang, X. Y. Wan, L. L. Zheng and C. Z. Huang, *Nanoscale*, 2014, **6**, 3868–3874.
32 P. Long, Y. Feng, C. Cao, Y. Li, J. Han, S. Li, C. Peng, Z. Li and W. Feng, *Adv. Funct. Mater.*, 2018, **28**, 1800791.
33 Y. Zhang, R. Yuan, M. He, G. Hu, J. Jiang, T. Xu, L. Zhou, W. Chen, W. Xiang and X. Liang, *Nanoscale*, 2017, **9**, 17849–17858.
34 X. Miao, X. Yan, D. Qu, D. Li, F. F. Tao and Z. Sun, *ACS Appl. Mater. Interfaces*, 2017, **9**, 18549–18556.
35 X. Miao, D. Qu, D. Yang, B. Nie, Y. Zhao, H. Fan and Z. Sun, *Adv. Mater.*, 2018, **30**, 1704740.
36 K. Jiang, S. Sun, L. Zhang, Y. Wang, C. Cai and H. Lin, *ACS Appl. Mater. Interfaces*, 2015, **7**, 23231–23238.
37 D. Chao, W. Lyu, Y. Liu, L. Zhou, Q. Zhang, R. Deng and H. Zhang, *J. Mater. Chem. C*, 2018, **6**, 7527–7532.
38 F. Yuan, Z. Wang, X. Li, Y. Li, Z. a. Tan, L. Fan and S. Yang, *Adv. Mater.*, 2017, **29**, 1604436.
39 B. B. Chen, M. L. Liu, C. M. Li and C. Z. Huang, *Adv. Colloid Interface Sci.*, 2019, **270**, 165–190.
40 B. B. Chen, Z. X. Liu, H. Y. Zou and C. Z. Huang, *Analyst*, 2016, **141**, 2676–2681.
41 L. Bu, T. Luo, H. Peng, L. Li, D. Long, J. Peng and J. Huang, *Microchim. Acta*, 2019, **186**, 675.
42 Y. Liu, S. Luo, P. Wu, C. Ma, X. Wu, M. Xu, W. Li and S. Liu, *Anal. Chim. Acta*, 2019, **1090**, 133–142.
43 J. Jana, H. J. Lee, J. S. Chung, M. H. Kim and S. H. Hur, *Anal. Chim. Acta*, 2019, **1079**, 212–219.
44 J. Jia, W.-J. Lu, L. Li, Y. Jiao, Y.-F. Gao and S.-M. Shuang, *Chin. J. Anal. Chem.*, 2019, **47**, 560–566.
45 Y. H. Yuan, Z. X. Liu, R. S. Li, H. Y. Zou, M. Lin, H. Liu and C. Z. Huang, *Nanoscale*, 2016, **8**, 6770–6776.